Supplementary Information

Modulating oxygen vacancy to simultaneously promote Pd atom stability and O activation over Pd/CeO$_2$ catalysts for enhancing catalytic efficiency and durability

Ke Tang, [a] Xiaoyang Liu, [a] Guofei Jiang,*[a] Ying Zhang, [a] Xiangyan Meng, [a] Jiangbo Lu,*[b] Hanyu Zhang, [a] Yiping Gao, [a] Zhengxing Qin, [c] and Feng Lin*[a]

[a]School of Chemistry and Chemical Engineering, Heze University, Heze, 274015, P. R. China

[b]School of Physics and Information Technology, Shaanxi Normal University, Xi'an, 710119, P. R. China

[c]State Key Laboratory of Heavy Oil Processing, College of Chemical Engineering, China University of Petroleum (East China), Qingdao, 266580, P. R. China

*E-mail: jianggf@hezeu.edu.cn, jblu10@snnu.edu.cn, linfeng@hezeu.edu.cn

Experimental Section

Chemicals

Cerium hexahydrate nitrate ($Ce(NO_3)_3·6H_2O$, 99.99%, Aladdin), sodium carbonate (Na_2CO_3, >99.8%, Adamas), palladium chloride ($PdCl_2$, 99%, Aladdin), ethanol (EtOH, AR, Adamas), sodium hydroxide (NaOH, >98%, Adamas).

Synthesis of CeO_2

CeO_2 supports were synthesized using a solvothermal method. The two kinds of $Ce(NO_3)_3.6H_2O$ solution (5 mL, 0.4 mol L^{-1}) and NaOH solution (35 mL, 7 mol L^{-1}) were mixed in a Teflon bottle under stirring for 30 min and heated to 100 °C for 24 h. After washing with deionized water and ethanol, samples were dried at 60 °C and calcined at 500 °C for 2 h with a heating rate of 2 °C min^{-1}.

Synthesis of Pd/CeO_2

50 mg CeO_2 supports were dispersed in 10 mL deionized water. After adjusting the pH ~9 by Na_2CO_3 aqueous solution (0.5 M), the calculated amounts of Pd (II) stock solution (0.5 wt%) were added into the suspension. After stirring for 1 h at room temperature, the products were washed with deionized water and ethanol. After drying at 60 °C, the products were calcinated at 700 °C under two kinds of calcination conditions, one of which was in tube furnace with a calcination rate of 2 °C min^{-1} (denoted as PdCe-NC700), and the second was in light-assisted heating furnace with a rapid temperature rise to 700 °C within 3.9 s (denoted as PdCe-TS700).

Characterization

Inductively coupled plasma optical emission spectrometry (ICP-OES) was performed on Thermo ICAP PRO to detect the metal contents. X-ray diffraction (XRD) was performed on Rigaku D/Max 2200PC diffractometer with Cu Kα radiation (λ = 0.15418). Transmission electron microscopy (TEM) was obtained on TALOS F200S G2. High-angle annular dark-field scanning transmission electron microscopy (HAADF-STEM) and energy-dispersive X-ray spectroscopy (EDX) mapping were conducted on FEI Titan cubed Themis G2 300 microscope operated at 300 kV equipped with probe aberration corrector and monochromator. Electron Paramagnetic Resonance (EPR) tests were carried out on Bruker ELEXSYS II at room temperature. N_2 adsorption-desorption was performed on BSD-PS4 apparatus to analyze the surface area and pore size of catalysts. X-ray photoelectron spectroscopy (XPS) was performed on ThermoFisher K-Alpha using Al-Kα radiation. All the binding energies were corrected by the C 1s peak at 284.8

eV.

Diffuse reflectance infrared Fourier-transform spectroscopy (DRIFT) spectra of CO adsorption were collected on Bruker Vertex 70 FTIR spectrometer equipped with a mercury cadmium telluride (MCT) detector. The catalysts were pretreated in pure Ar at 200 ^oC for 30 min. After cooling to 30 ^oC, background spectra were collected, and then the flowing gas was switched to 2% CO/Ar for 30 min. Upon exposure to pure Ar, the spectra were recorded with 4 cm^{-1} resolution.

H_2 temperature-programmed reduction (H_2-TPR) were performed on BSD-Chem C200 equipped with a thermal conductivity detector (TCD). 25 mg catalysts were placed in a U-shaped quartz reactor and pretreated in pure Ar at 200 ^oC for 30 min. After cooling to 30 ^oC, the flowing gas was switched to 10% H_2/Ar, and then the H_2 consumption were recorded at the temperature region 30 ^oC-300 ^oC.

Catalytic activity measurements

CO oxidation reaction was performed in a continuous flow fixed-bed microreactor under atmospheric pressure. 25 mg catalysts were placed in a reactor with a gas mixture of 1% CO, 10% O_2, and 89% N_2 at a rate of 60 ml min^{-1}. Space velocity was 140000 ml h^{-1} g^{-1}. The effluent gas compositions were monitored by an infrared gas analyzer (Gasboard-3100) equipped with a thermal conductivity detector (TCD).

Computational Method

Calculation of density functional theory DMOL3 package based on density functional theory in Materials Studio was utilized for calculation.[1, 2] The main calculation was performed by generalized gradient approximation (GGA) and Perdew-Burke-Ernzerh (PBE) of exchange-correlation potential. Grimme method was used for DFT-D correction. The k-point sampling was done with Monkhorst-Pack grid with grid number as 5×5×1. The total energy was calculated by self-consistent iteration (SCF) method, and 0.005 Ha smearing was also used.

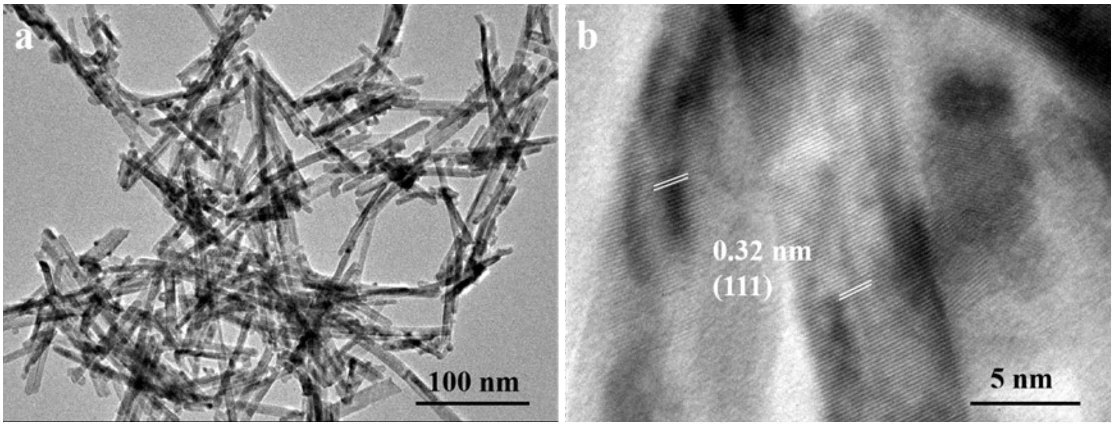

Fig. S1 HRTEM images of CeO_2 nanorods.

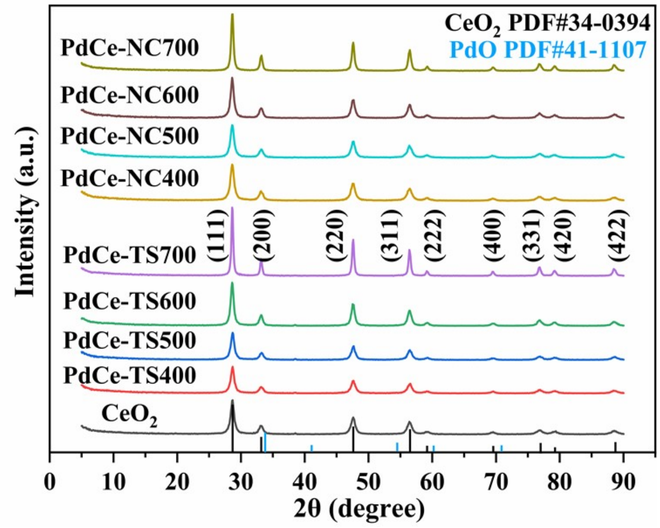

Fig. S2 XRD patterns.

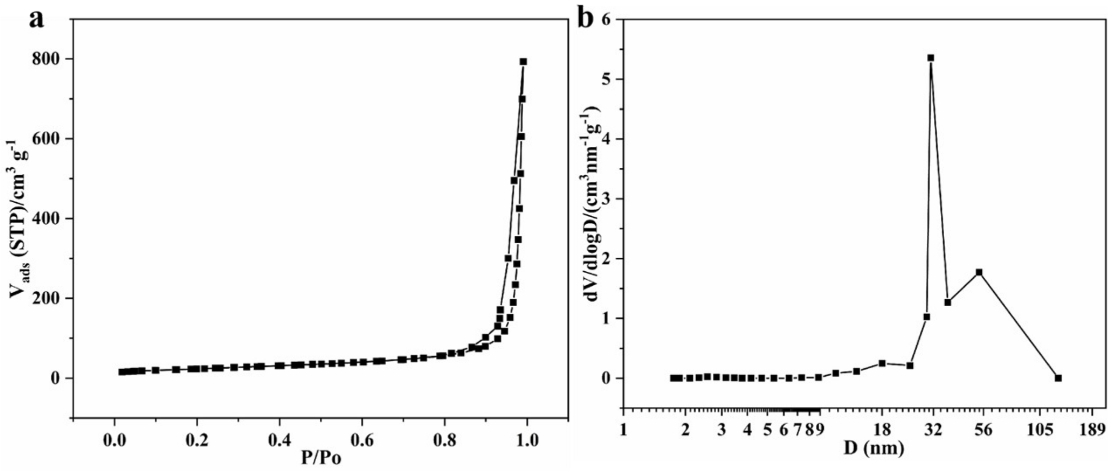

Fig. S3 Nitrogen adsorption-desorption isotherms (a) and pore size distribution plots (b) of CeO_2 nanorods.

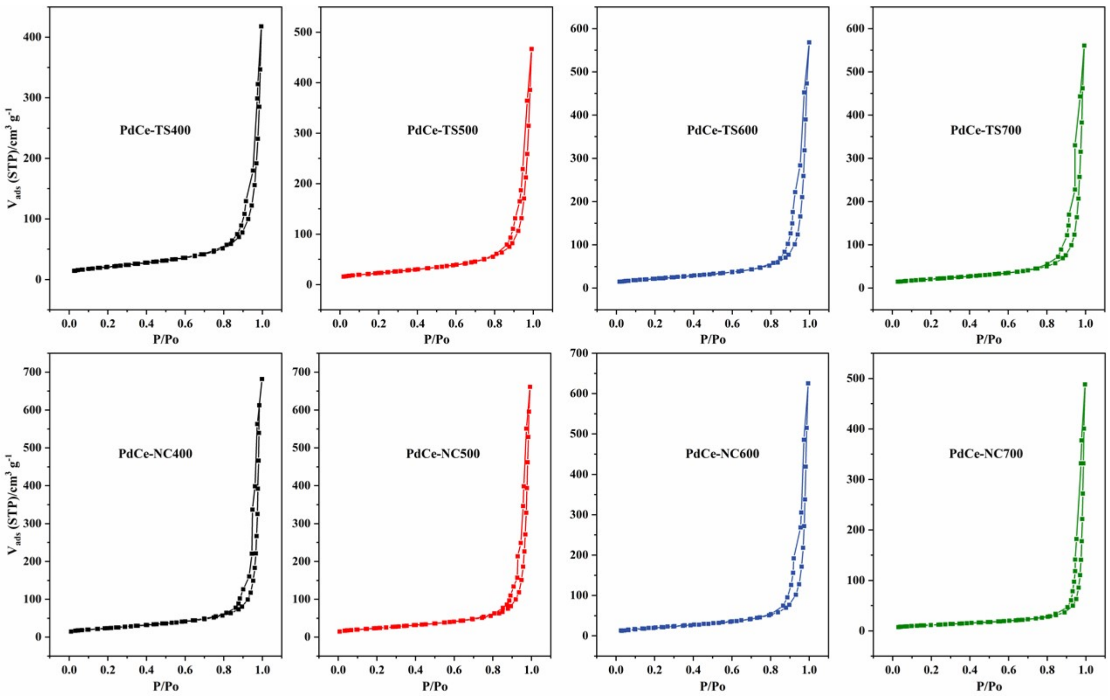

Fig. S4 Nitrogen adsorption-desorption isotherms.

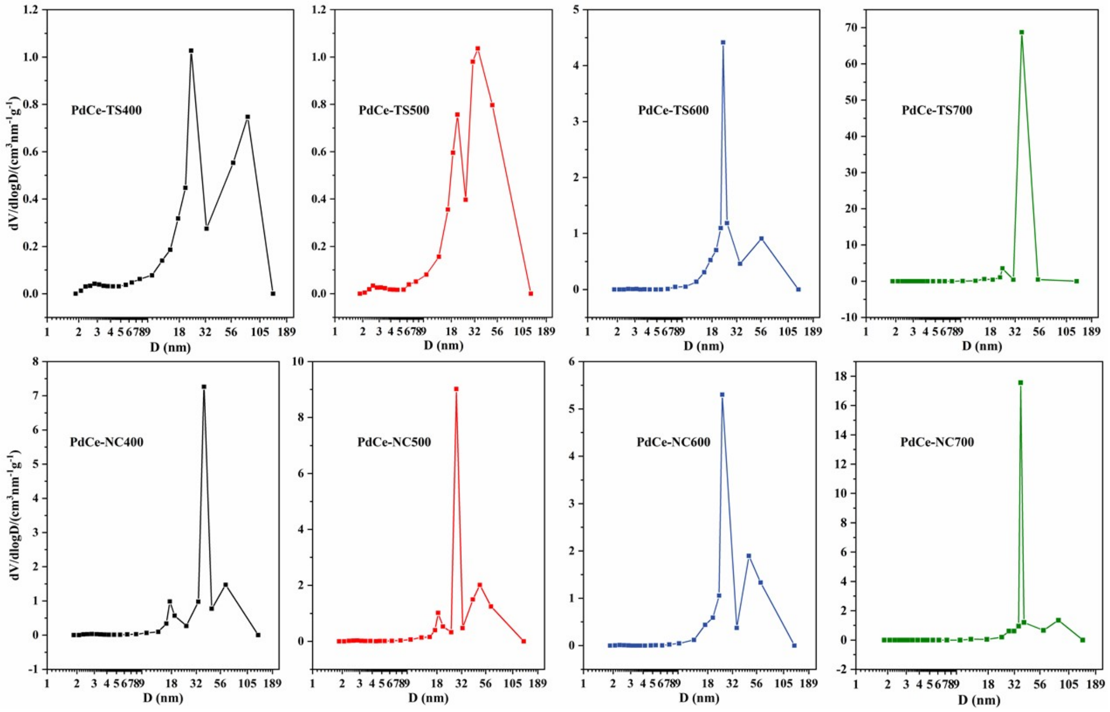

Fig. S5 Pore size distribution plots.

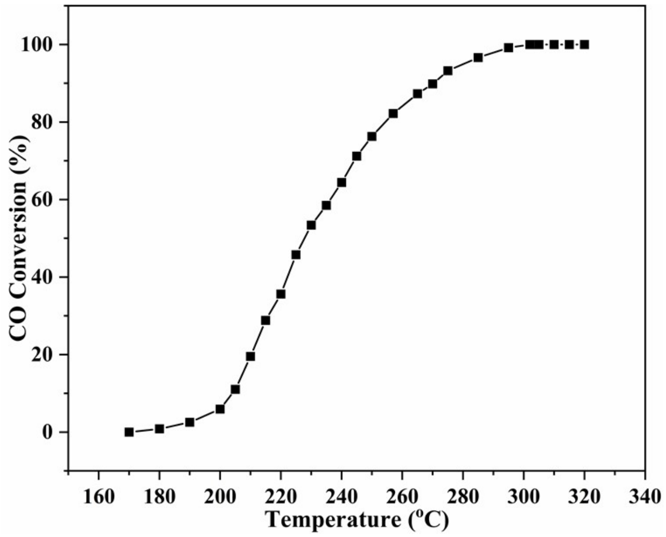

Fig. S6 CO oxidation curve of CeO_2 nanorods.

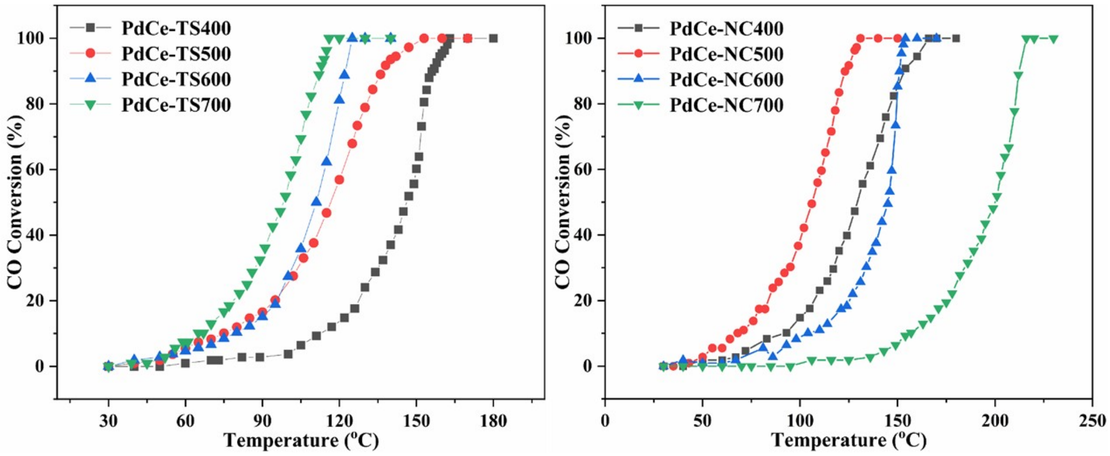

Fig. S7 CO oxidation curves.

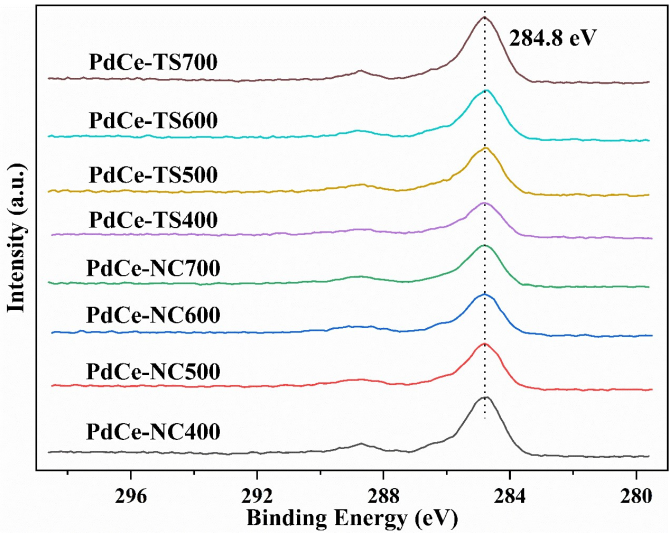

Fig. S8 C 1s spectra.

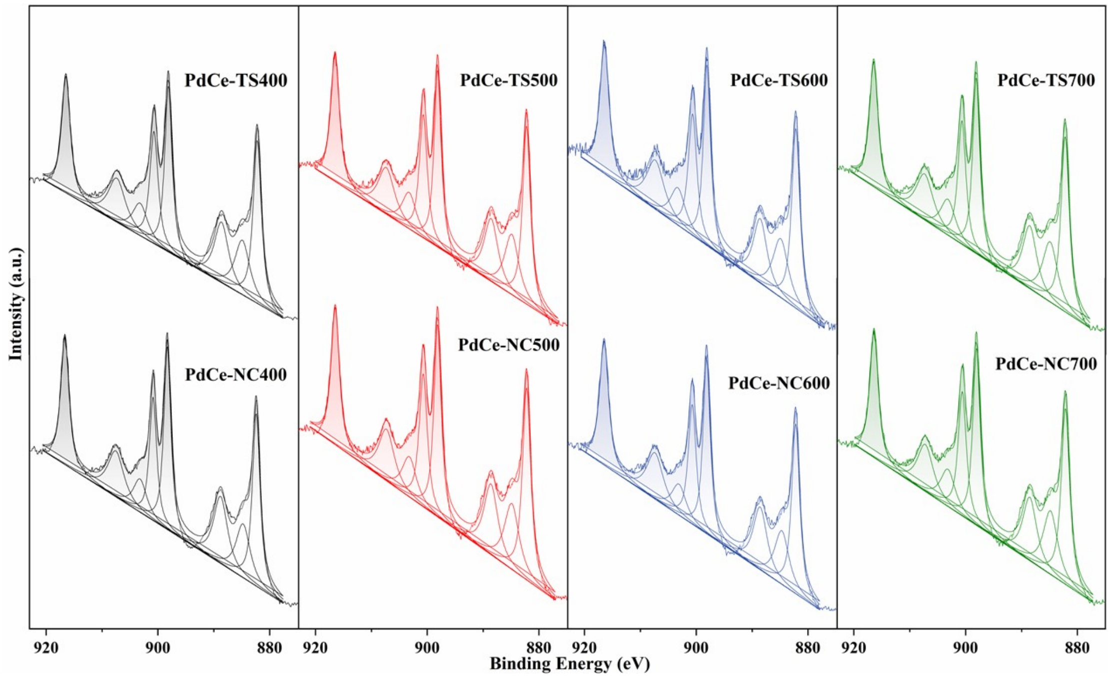

Fig. S9 Ce 3d spectra.

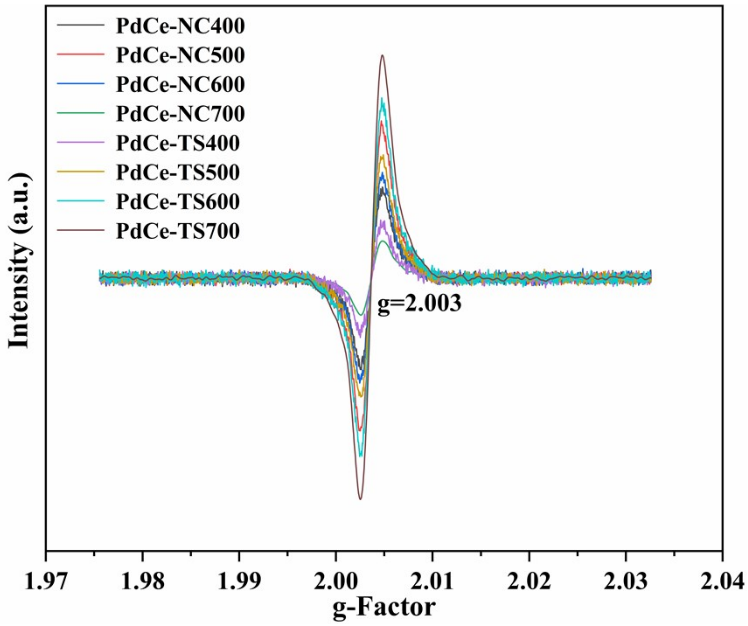

Fig. S10 EPR profiles.

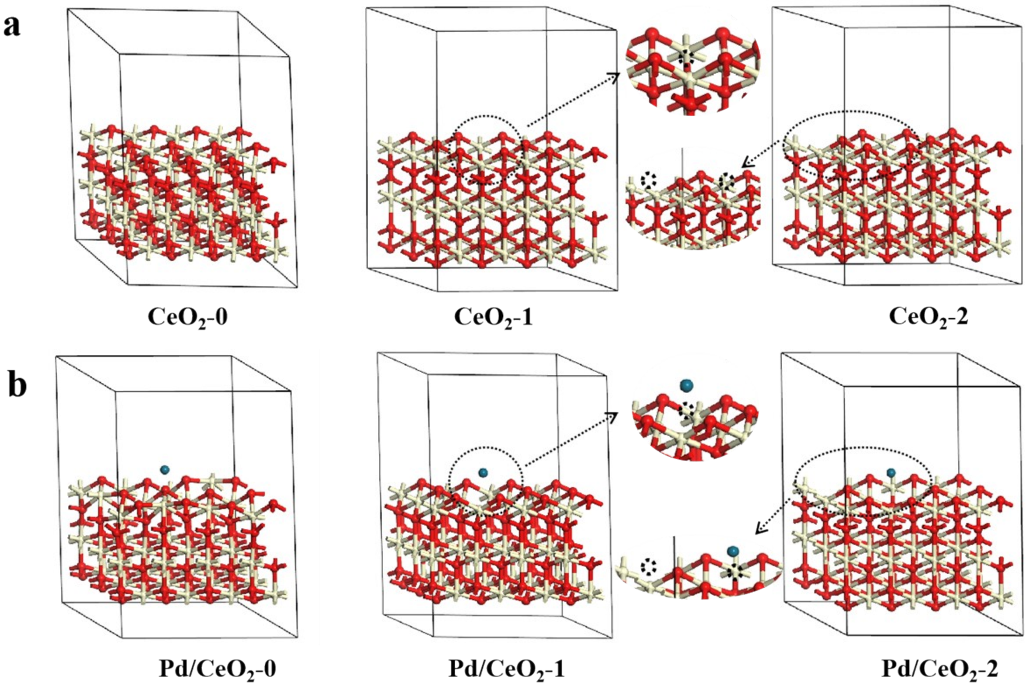

Fig. S11 (a) CeO$_2$-x models and (b) Pd/CeO$_2$-x models. x represents the amount of oxygen vacancy, with the value as 0, 1, 2. The black circles were corresponding to oxygen vacancies. a=15.4128 Å, b=11.4974 Å, c=22.7419 Å and α=90.0829°, β=90.2030 °, γ=120.1994 °. The Ce, O and Pd atoms are shown as white, red and blue balls, respectively.

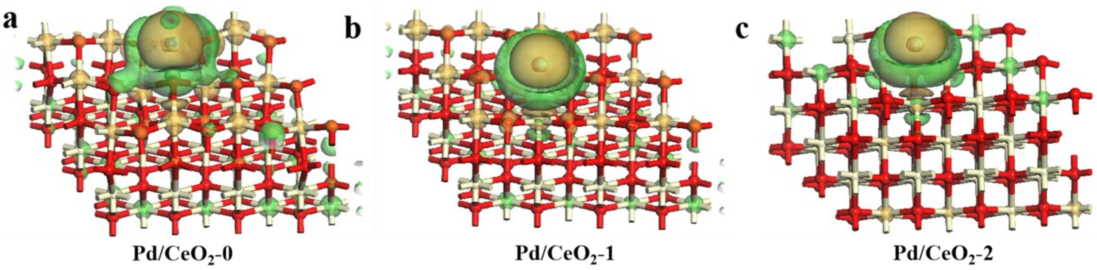

Fig. S12 Differential charge density diagram for Pd/CeO$_2$-0, Pd/CeO$_2$-1 and Pd/CeO$_2$-2 models, in which green and yellow isosurfaces represent accumulation and loss of net electron, respectively, and the isosurface value was 0.015 electron/Å^3. The Ce, O and Pd atoms are shown as white, red and blue balls, respectively.

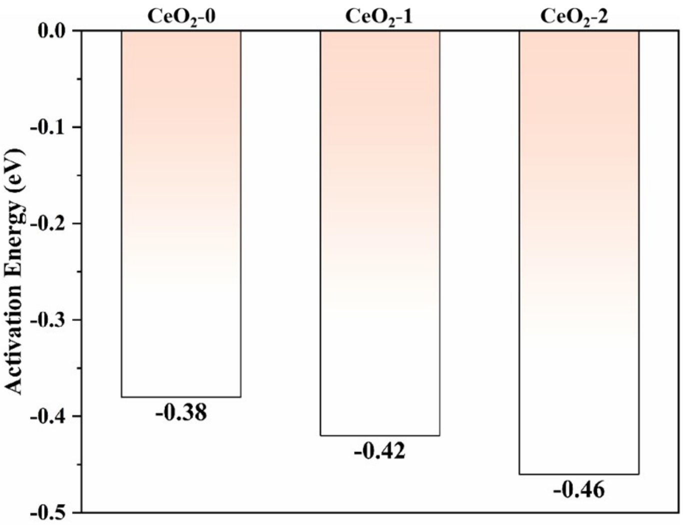

Fig. S13 Oxygen adsorption energy of CeO$_2$-0, CeO$_2$-1 and CeO$_2$-2 models.

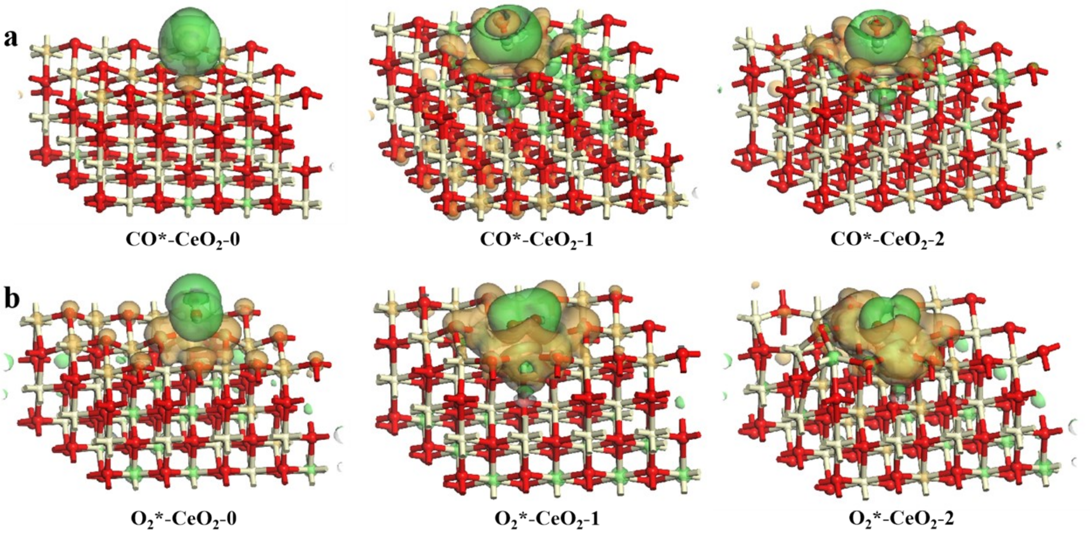

Fig. S14 Differential charge density diagram for CeO$_2$-0, CeO$_2$-1 and CeO$_2$-2 models, in which green and yellow isosurfaces represent accumulation and loss of net electron, respectively, and the isosurface value was 0.015 electron/Å^3. The Ce, O, Pd and C atoms are shown as white, red, blue and gray balls, respectively.

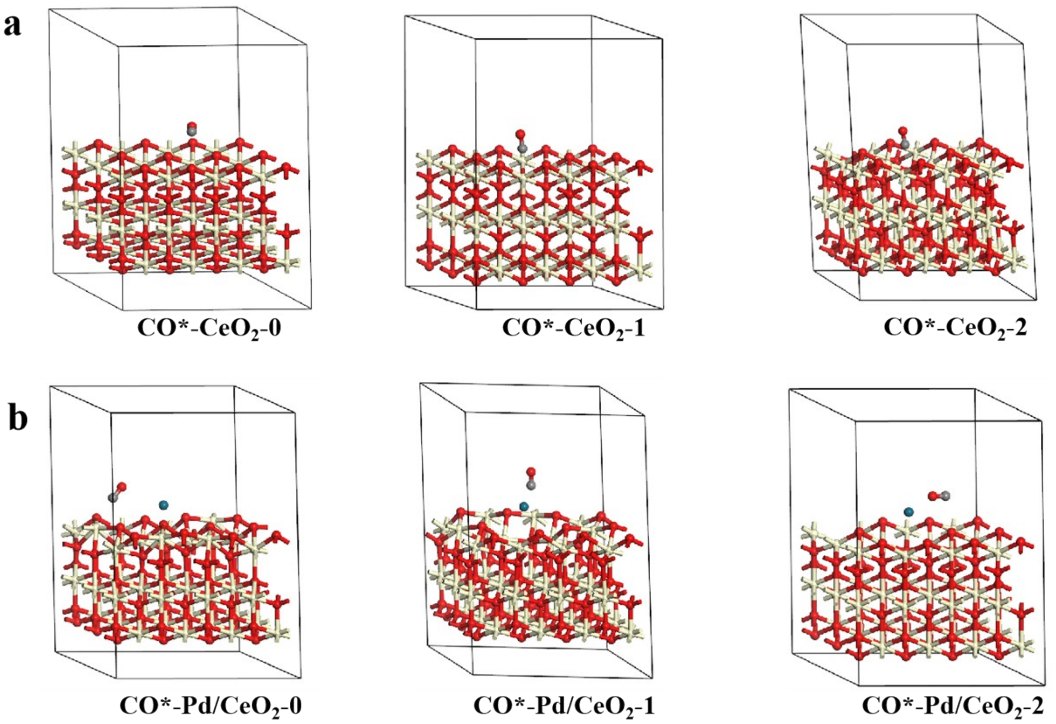

Fig. S15 **(a) CO*-CeO$_2$-x models and (b) CO*-Pd/CeO$_2$-x models. x represents the amount of oxygen vacancy, with the value as 0, 1, 2. The Ce, O, Pd and C atoms are shown as white, red, blue and gray balls, respectively.**

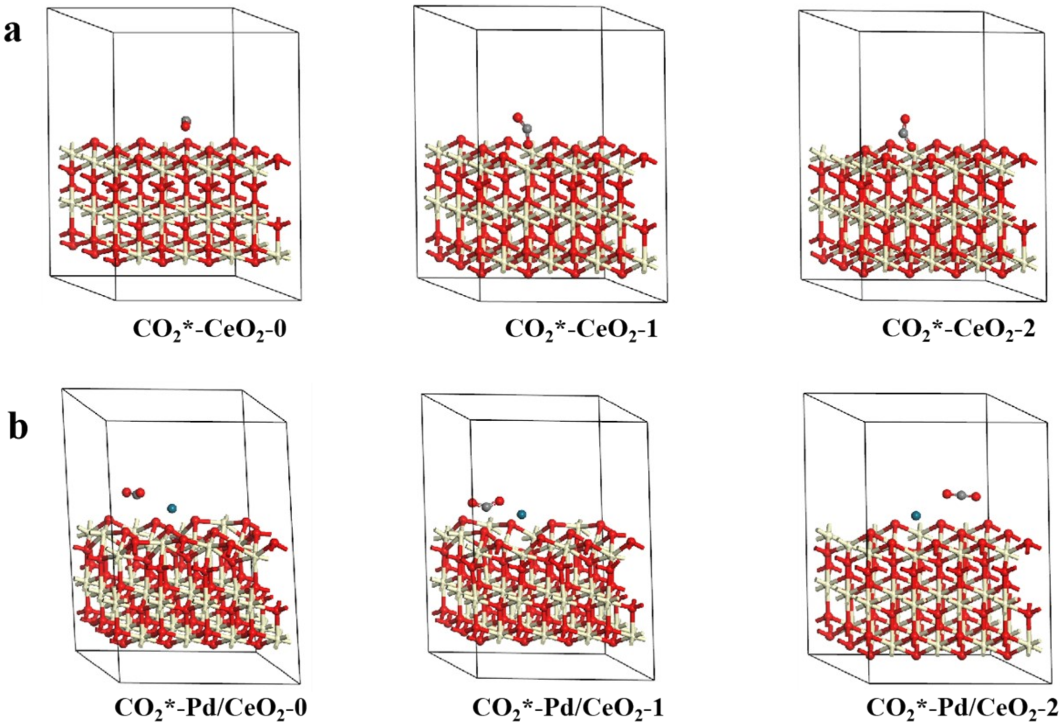

Fig. S16 **(a) CO$_2$*-CeO$_2$-x models and (b) CO$_2$*-Pd/CeO$_2$-x models. x represents the amount of oxygen vacancy, with the value as 0, 1, 2. The Ce, O, Pd and C atoms are shown as white, red, blue and gray balls, respectively.**

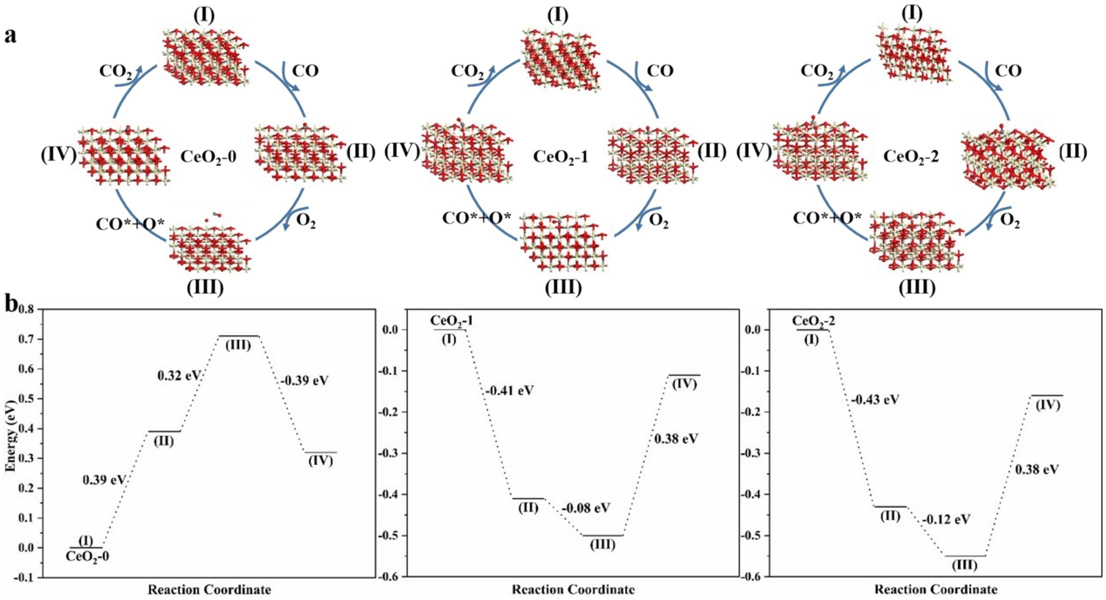

Fig. S17 (a) CO oxidation schemes for CeO$_2$-0, CeO$_2$-1 and CeO$_2$-2 models. CO and O$_2$ adsorption (step 1 and 2), CO* interacts with dissociatively adsorbed O$_2$ (O*, step 3), and CO$_2$ desorption (step 4). (b) Reaction energy diagram. The Ce, O and C atoms are shown as white, red and gray balls, respectively.

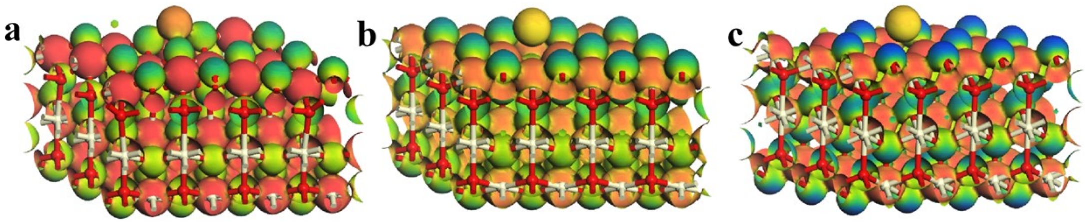

Pd/CeO$_2$-0 **Pd/CeO$_2$-1** **Pd/CeO$_2$-2**

Fig. 18 The electrostatic potential distribution of (a) Pd/CeO$_2$-0, (b) Pd/CeO$_2$-1 and (c) Pd/CeO$_2$-2.

Based on the experimental and theoretical study, we can conclude the role of Pd single atom and oxygen vacancy. Firstly, the low binding energy facilitates the adsorption of the CO molecules on Pd. Then, the abundant electrons donated from oxygen vacancies further activate CO and weaken the CO-poisoning effect. Additionally, the abundant oxygen vacancies can facilitate the activation of O$_2$, making CO oxidation easier. The superior ability for CO$_2$ removal simultaneously accelerated the overall reaction.

Table S1. ICP-OES data, surface area, total pore volume and pore size of catalysts

Sample	Pd Loading ICP-OES (wt%)	Surface Area (m^2/g)	Total Pore Volume (cm^{-3}/g)	Pore Size (nm)
PdCe-TS400	0.51	74.53	0.55	29.94
PdCe-TS500	0.52	81.61	0.70	34.50
PdCe-TS600	0.49	79.08	0.78	39.41
PdCe-TS700	0.51	75.00	0.80	42.55
PdCe-NC400	0.49	85.64	0.99	46.34
PdCe-NC500	0.50	85.79	0.97	45.42
PdCe-NC600	0.53	75.95	0.86	45.60
PdCe-NC700	0.51	42.31	0.62	58.87
CeO_2	--	84.45	1.19	56.65

Table S2. Catalytic activity data of catalysts

Sample	CO Conversion	
	T_{50}	T_{100}
PdCe-TS400	146	163
PdCe-TS500	117	153
PdCe-TS600	111	125
PdCe-TS700	98	116
PdCe-NC400	129	166
PdCe-NC500	107	131
PdCe-NC600	145	154
PdCe-NC700	200	216
CeO_2	228	302

T_{50} and T_{100} are corresponding to CO conversion at 50% and 100%, respectively.

Table S3. Peak position and H_2 consumption of H_2-TPR

Sample	H_2-TPR			
	α		α′	
	Position (°C)	H_2 (mmol/g)	Position (°C)	H_2 (mmol/g)
PdCe-TS400	92	0.51	148	0.83
PdCe-TS500	85	0.50	150	0.50
PdCe-TS600	86	0.94	140	0.66
PdCe-TS700	66	1.43	--	--
PdCe-NC400	85	0.49	154	0.56
PdCe-NC500	70	0.77	155	0.14
PdCe-NC600	75	0.52	154	0.64
PdCe-NC700	89	0.19	150	0.40

Table S4. Quantification of H_2-TPR data and XPS data

Sample	H_2 (total) (mmol/g_{cat})	H_2/Surface Area (μmol/m^2)	H_2 (Pd^{2+})/ H_2 (total) (%)	$OH/O^{2-}+OH+H_2O$ (%)	$Ce^{3+}/Ce^{3+}+Ce^{4+}$ (%)
PdCe-TS400	1.34	6.84	38.05	23.40	17.46
PdCe-TS500	1.00	6.12	50.00	24.01	17.77
PdCe-TS600	1.60	11.88	58.75	25.55	17.81
PdCe-TS700	1.43	18.80	100	30.46	18.18
PdCe-NC400	1.05	5.72	46.66	22.92	16.23
PdCe-NC500	0.91	8.97	84.61	26.33	17.98
PdCe-NC600	1.16	6.84	44.82	22.41	16.14
PdCe-NC700	0.59	4.49	32.20	21.32	14.24

Table S5. Binding energies of catalysts

Sample	Binding Energy (eV)					
	Ce 3d				O 1s	Pd 3d
	v′	u′	v v″ v‴	u u″ u‴		
PdCe-TS400	884.8	903.1	882.2 888.6 898.1	900.6 907.3 916.4	529.0 531.4	337.6 343.0
PdCe-TS500	884.8	903.2	882.2 888.5 898.1	900.7 907.3 916.5	529.1 531.8	337.7 343.0
PdCe-TS600	884.9	903.2	882.1 888.5 898.0	900.6 907.3 916.4	529.1 531.6	337.7 343.0
PdCe-TS700	884.9	903.2	882.1 888.5 898.0	900.6 907.3 916.4	529.1 531.8	337.7 343.1
PdCe-NC400	884.7	903.2	882.4 888.8 898.3	900.8 907.5 916.6	529.1 531.4	337.6 342.8
PdCe-NC500	884.8	903.2	882.2 888.6 898.1	900.7 907.3 916.4	529.1 531.6 533.1	337.6 342.9
PdCe-NC600	884.6	903.1	882.2 888.5 898.1	900.7 907.3 916.5	529.0 531.4	337.6 342.9
PdCe-NC700	884.7	903.1	882.1 888.4 898.0	900.6 907.1 916.3	529.0 531.5	337.3 342.6

References

[1] B. Delley, An all‐electron numerical method for solving the local density functional for polyatomic molecules, J. Chem. Phys. 92(1) (1990) 508-517. https://doi.org/10.1063/1.458452.

[2] B. Delley, A scattering theoretic approach to scalar relativistic corrections on bonding, Int. J. Quantum Chem. 69(3) (1998) 423-433. https://doi.org/https://doi.org/10.1002/(SICI)1097-461X(1998)69:3<423::AID-QUA19>3.0.CO;2-2.